Geometric frustration induces the transition between rotation and counterrotation in swirled granular media

Lisa M. Lee,[1] John Paul Ryan,[2] Yoav Lahini,[3] Miranda Holmes-Cerfon,[4,*] and Shmuel M. Rubinstein[1,*]

[1]*John A. Paulson School of Engineering and Applied Sciences, Harvard University, Cambridge, Massachusetts 02138, USA*
[2]*Department of Computer Science, Cornell University, Ithaca, New York 14850, USA*
[3]*Raymond and Beverly Sackler School of Physics and Astronomy, Tel Aviv University, Tel Aviv, Israel*
[4]*Courant Institute of Mathematical Sciences, New York University, New York, New York 10012, USA*

Granular material in a swirled container exhibits a curious transition as the number of particles is increased: At low densities, the particle cluster rotates in the same direction as the swirling motion of the container, while at high densities it rotates in the opposite direction. We investigate this phenomenon experimentally and numerically using a corotating reference frame in which the system reaches a statistical steady state. In this steady state, the particles form a cluster whose translational degrees of freedom are stationary, while the individual particles constantly circulate around the cluster's center of mass, similar to a ball rolling along the wall within a rotating drum. We show that the transition to counterrotation is friction dependent. At high particle densities, frictional effects result in geometric frustration, which prevents particles from cooperatively rolling and spinning. Consequently, the particle cluster rolls like a rigid body with no-slip conditions on the container wall, which necessarily counterrotates around its own axis. Numerical simulations verify that both wall-disk friction and disk-disk friction are critical for inducing counterrotation.

From hurricanes to bacterial swarms, the emergence of system-scale circulation from local interactions and local driving is a phenomenon exhibited on many scales and in many different physical systems. In two-dimensional (2D) turbulence, vorticity at the small injection scale may cascade to larger scales, stabilizing into a single system-scale vortex [1,2]. Analogous behavior is observed in an active fluid of spinners flowing though a lattice of annular channels and driven by a magnetic field, which breaks time-reversal symmetry. This active liquid develops sound modes that propagate along the boundary, generating global circulation [3]. Finally, dense suspensions of self-propelled bacteria in confinement also lead to the spontaneous formation of stable circulation along the container walls [4,5]. In all of these systems, rotation is actively or passively injected locally, and interactions between the local units ultimately lead to global circulation of the entire system.

There is no need to go to very complex systems to observe the nontrivial emergence of system-size circulation. A handful of marbles swirled in a teacup exhibits similar dynamics. When there are only a few marbles in the container, they form a line that rolls along the container wall at the frequency of the circular translations ("snake" mode [6]). When a couple more marbles are added, they form a cluster that sloshes periodically around the container, its individual marbles repeatedly cramming against the wall at the outer edges of the swirl before flowing freely through the rest of the container. This sloshing marble ensemble rotates about its own center of mass in the same direction as the container, much like wine swirling in a glass. When even more marbles are added, the monolayer of marbles will continue to periodically slosh around the container, but, curiously, above a critical marble density the pack reverses to counterrotation, or to rotating in the direction *opposite* to that of the container [7]. This transition to counterrotation is startling, because the angular momentum of the marbles in their own reference frame changes sign with the addition of a couple marbles and is ultimately opposite that of the hand which forces them. The transition is not restricted to marbles in a teacup but can be observed in a variety of shaken containers filled with granular material, from vibration mills for grinding industrial materials [8] to baby rattles.

Such a simple and ubiquitous phenomenon demands an explanation, yet, while it has been studied empirically [6,7,9–11], there is still no clear understanding of the minimal ingredients necessary for it to occur. We propose to understand this phenomenon via analogies to a single rigid body and a fluid in a swirled container. A single rigid body in a swirled container with no-slip boundary conditions will roll commensurately on the wall (akin to one gear inside another), rotating about its own center of mass in the opposite direction as the container. One sees similar behavior for a pancake rolling on the edge of a swirled frying pan. In contrast, a rigid body with perfect-slip boundary conditions (as if the pancake were in a bath of melted butter) would receive no torque from the boundary and hence experience no overall sense of rotation. Finally, a fluid will rotate in the same direction as the container is swirled, also to varying degrees based on its slip conditions with the container wall. Thus, the rotation

*Corresponding authors:
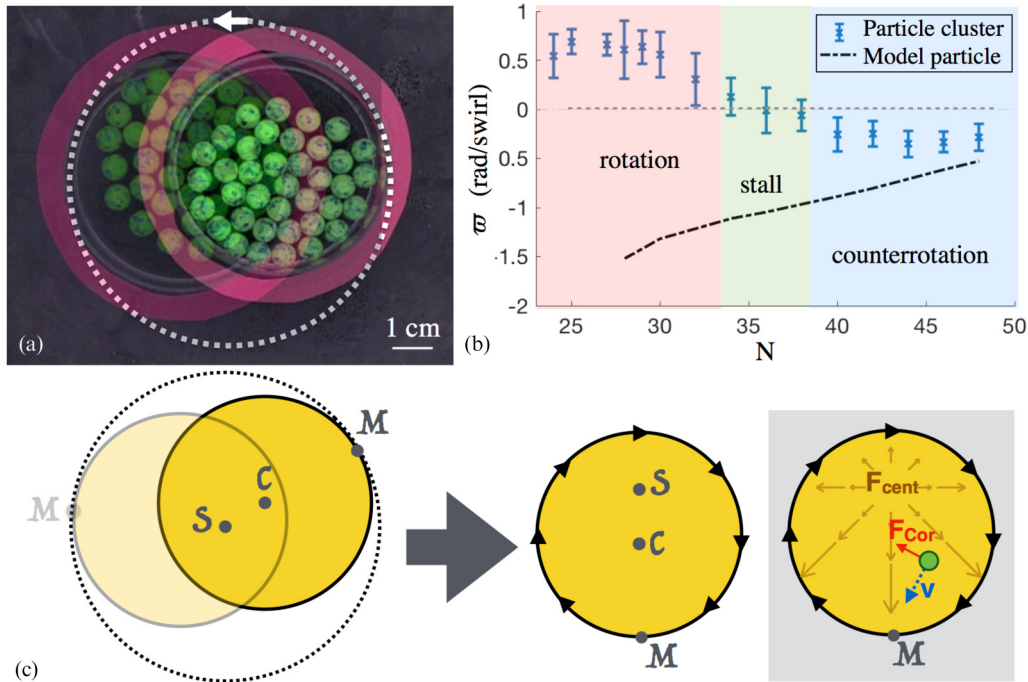holmes@cims.nyu.edu; shmuel@seas.harvard.edu

FIG. 1. (a) Raw image of experimental particles in a swirling container, and the same container at a later time after it has translated through roughly half its circular trajectory. The white dotted line represents the outermost points of the container during its trajectory. The container does not rotate in the laboratory frame. (b) The mean angular velocity (ϖ) of the particle cluster about its own center of mass for different particle counts N. ϖ is reported as how many radians the cluster gains on each swirling cycle of the dish. As N increases, the cluster transitions from rotation to stalling to counterrotation. Black dashed line indicates the angular velocity of a theoretical single particle or pancake, with perimeter matching that of the cluster, if it were perfectly rolling along the wall. (c) The M frame rotates with the container such that the point (left, labeled "M") on the container's boundary furthest from the center of swirling is always positioned at the bottom in the M frame (middle and right). As a result, the walls of the container in the M frame appear to be rotating clockwise, as depicted by the black arrows. Also shown are the point S, center of swirling, and the point C, center of the container. The rightmost M-frame diagram depicts the centrifugal force field (F_{cent}, brown) as well as the Coriolis force (F_{Cor}, red) associated with a particle (green) with indicated velocity (v, blue).

behavior of a single body in a swirled container depends on its own rigidity as well as its slip interactions with the wall. For granular systems composed of many interacting bodies, the fluidity and boundary interactions are not material constants but are emergent dynamic properties [12–16], determined by the friction between the particles as well as the friction with the container wall.

Here, we experimentally and numerically investigate the dynamics of swirling particles with the goal of identifying the minimal physical factors that facilitate the transition from rotation to counterrotation as the number of particles is increased. We show that the critical control parameter for counterrotation is the particle cluster's effective slip with the wall, which arises from friction. Although the individual particles' friction coefficient with the wall does not depend on the number of particles, the effective boundary condition of the particle cluster does and can change from perfect slip to perfect stick as the number of particles is increased. Our experimental observations suggest that friction between the particles prevents densely packed particles from cooperatively rolling and spinning, causing the particle cluster to rigidify and roll on the wall as a whole, ultimately resulting in counterrotation. Finally, we numerically simulate the swirling system and find that if either interparticle friction or particle-wall friction is set to zero, the system rotates at the same frequency at all densities and never

transitions to counterrotation, verifying that friction is critical for counterrotation.

I. EXPERIMENTAL RESULTS

Experimentally, the transition from rotation to counterrotation of swirling particles is observed upon a RotoMix orbital table performing circular translations, without rotation, of angular velocity $\omega = 11.81$ rad/s and amplitude 1.15 cm. The mounted circular container, 5.1 cm in diameter, with a vertical edge is partially filled with a monolayer of N (ranging from 24 to 48) plastic spheres (mass $m = 0.12$ g and diameter 6 mm) and imaged from above using a stationary Sony RX100 IV camera at 960 fps, as shown for two typical images in Fig. 1(a). We call the collection of particles a "cluster" and measure its average angular velocity ϖ by the average angular velocity of the particles about the cluster's center of mass: $\varpi = \frac{1}{T-\Delta t} \frac{1}{N} \sum_{t=\Delta t}^{T} \sum_{i=1}^{N} \varpi_i(t)$. Here, T is the total number of frames and $\varpi_i(t)$ is particle i's instantaneous angular velocity about the cluster's center of mass at time t: $\varpi_i(t) = \frac{1}{\Delta t}[\arctan(\frac{y(t,i)-y_{c.m.}}{x(t,i)-x_{c.m.}}) - \arctan(\frac{y(t-\Delta t,i)-y_{c.m.}}{x(t-\Delta t,i)-x_{c.m.}})]$. Here, $x_{c.m.}$ and $y_{c.m.}$ refer to the x and y coordinates of the center of mass of all particles.

Under these conditions, the average angular velocity ϖ crosses zero and transitions between rotation and counterrotation at roughly 36 particles, as shown in Fig. 1(b) and

the Supplemental Material [17]. For $N > 36$, the cluster counterrotates ($\varpi < 0$), and for even higher values of N, the average angular velocity reaches a minimum and then increases slightly for the largest values of N.

A. The M frame

Further analyzing the data in the laboratory frame is a challenge since the particles experience a rotating time-dependent force from the circular translations of the swirling container; thus, the particles slosh around the container with no apparent steady state (see the Supplemental Material [17]). Therefore, it is illuminating to analyze the data in a frame of reference where the external forces are steady [10]. Consider a rotating frame, which rotates at the angular velocity ω of the container, about an axis at the center S of the swirling orbit. In this frame of reference, the container's translational velocity is zero and it rotates around its own center C at a constant angular speed $-\omega$. This frame of reference is equivalent to centering our camera above the center of the container and rotating it such that S is stationary, keeping the boundary point furthest from S at the bottom; hereafter, we refer to this point as the point M, as shown in Fig. 1(c). In this frame of reference, there are two external forces acting on all particles: the centrifugal force, which points radially away from S with magnitude at a point x equal to $m\omega^2|x - S|$, and the Coriolis force, which points perpendicularly to the right of the particle's velocity vector v, with magnitude $2m|v|\omega$ ([18], Sec. 39). More details on this change of coordinate system are provided in the Supplemental Material [17]. Within the container, the centrifugal force pushes the particles outward to the boundary, and then its tangential component pushes particles toward M. At the boundary, the particles are also dragged clockwise due to friction with the moving container wall. We call the original frame of reference the laboratory frame and the rotating frame of reference the M frame. The latter terminology is borrowed from Kumar *et al.* [10], who used this frame of reference to study granular particles on the edge of a swirling cylinder.

In the M frame, the system can reach a steady state because the external forces on it are constant in time. Experimentally, our system appears to be at steady state when averaged over typical fluctuations [Supplemental Material [17] and Fig. 2(a)], characterized by a steady particle density pattern and a steady circulation pattern as shown in Figs. 2(b) and 2(c). The steady state in our system bears a striking resemblance to the steady state in a rotating drum. In the rotating drum, gravity pulls beads to the bottom of the drum, where they form a compact cluster, and then the wall of the drum drags the bead cluster upward, until it liquefies and the beads avalanche back to the bottom of the drum, continuing the cycle. In the M frame, the force of gravity is replaced by the centrifugal force, which both push particles toward point M at the bottom. Additionally, the M frame introduces the Coriolis force that the rotating drum lacks, resulting in the beads tending to the left of the container.

In the M frame, all particles follow clockwise trajectories within the container while passing between two distinct spatial regions: a dense, "pinned" region (solid-like), and a sparse, "loose" region (liquid-like), as shown in Fig. 2(a) and
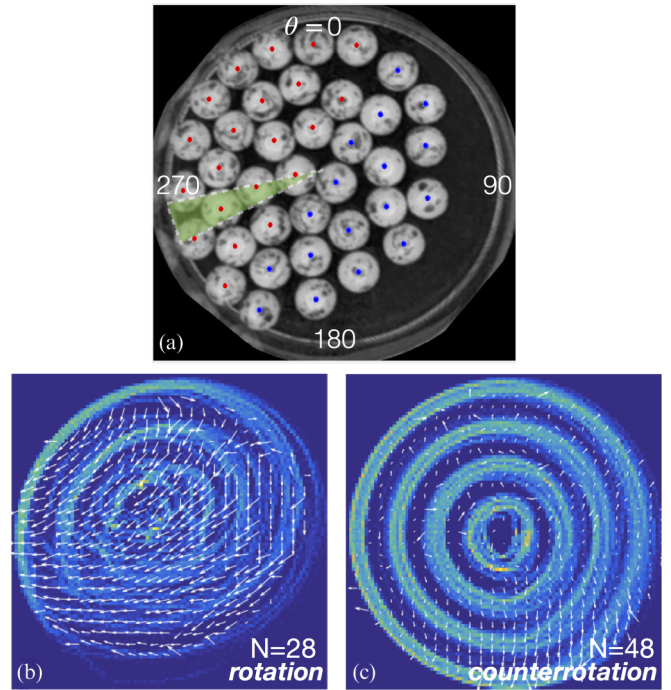

FIG. 2. (a) Sample experimental image in the M frame, with pinned (red) and loose (blue) region particle centers labeled. A sample angular slice interrogation area is highlighted in green. The angular slice slides around the entire container during analysis; the major angular positions θ are denoted on the edge of the container. (b) Density histogram of the particles for a rotation case at low $N = 28$. The white arrows denote the average local particle velocity deviation from the velocity of the underlying container. (c) Same as panel (b), but for counterrotation at high $N = 48$. The coherent pinned region (top left on the container) grows in size with increasing N, while the loose region shrinks in size. The particles perform clockwise trajectories around the container while passing between the pinned and loose regions in a cyclic manner.

calculated in the Supplemental Material [17]. In the pinned region, the particles are packed in layers against the moving wall and move as a rigid structure, whereas in the loose region the particles perform less constrained trajectories as they cross the container, as shown in Fig. 2(b). When a particle in the loose region transitions to the pinned region, it undergoes multiple collisions before settling into a trajectory parallel to the container's edge. Increasing N also increases the number of collisions a particle experiences, causing it to enter the pinned region earlier in its cycle and subsequently increasing the size of the pinned region. For all values of N, particles exit the pinned region and detach from the rigid structure at the same location. Once loose, a particle experiences centrifugal ($0-460\,\mathrm{cm/s^2}$) and Coriolis ($0-200\,\mathrm{cm/s^2}$) forces and accelerates as it traverses the loose region. Multiple collisions at the end of the loose region pin the particle and this cycle continues.

Individual particles circulate between these two regions and on average the particle cluster rotates in the same clockwise direction as the container in the M frame, shown for two typical examples in Figs. 2(b) and 2(c). Importantly, the cluster's angular velocity in the M frame, ϖ_M, is related to its

angular velocity in the laboratory frame as

$$\varpi_M = \varpi - \omega. \tag{1}$$

Therefore, counterrotation in the laboratory frame ($\varpi < 0$) corresponds to the particle cluster rotating faster than the dish in the M frame ($|\varpi_M| > \omega$).

B. Minimal model: Rigid ball in a swirled container

At this point, it is insightful to consider a minimal model for our swirling system: a single rigid ball of radius R_{ball} swirled in a container of radius R_{cont} (Supplemental Material [17]). A steady-state for the ball in the M frame occurs when it is near the bottom left of the container (near M), rotating at constant angular velocity ϖ_b with the torque along the frictional boundary balancing the centrifugal force. If we define a dimensionless parameter $\gamma = \frac{|\varpi_b|}{\omega}$, then by (1), $\gamma < 1$ corresponds to rotation in the laboratory frame and $\gamma > 1$ corresponds to counterrotation. The value of γ depends on the slip conditions between the ball and the container wall, which interpolate between two limiting cases: perfect no-slip (strong friction) and perfect slip (no friction). When friction is strong, the ball rolls commensurately on the wall of the container without slipping, and $\gamma = \gamma_c = \frac{R_{\mathrm{cont}}}{R_{\mathrm{ball}}}$. Since $R_{\mathrm{cont}} > R_{\mathrm{ball}}$, the ball thus counterrotates in the laboratory frame. Conversely, when there is no friction, the ball cannot rotate at all due to perfect slip boundary conditions and $\gamma = 0 < 1$, corresponding to rotation. In between the two extremes, the degree of wall slip can be measured by a slip parameter $s = \frac{\gamma}{\gamma_c} = \frac{\varpi_M}{\omega} \frac{R_{\mathrm{ball}}}{R_{\mathrm{cont}}}$, which varies from $s = 0$ for perfect slip conditions, to $s = 1$ for perfect no-slip conditions.

C. Particle cluster behavior

While the single-particle model captures much of why a swirled particle cluster can either rotate or counterrotate, the details are more subtle since an ensemble of particles rarely behaves exactly like a single rigid object. Even in the M frame, where the dynamics are in steady state, the instantaneous angular velocity of any single particle $\varpi_i(t)$ depends on where it is in the dish, as shown in Fig. 3(a). It is therefore more appropriate to refer to a particle's instantaneous velocity as $\varpi_i(\theta)$. The change in $\varpi_i(\theta)$ with θ can largely be characterized by the loose and pinned regions. In the loose region, the value of $\varpi_i(\theta)$ increases and decreases in a quantitatively similar manner for all values of N, with the only difference being the location on the dish at which this peak occurs. However, in the pinned region, the average value of $|\varpi_i(\theta)|$ consistently increases with increasing N. Therefore, the pinned region is the major contributor to the different behaviors seen across varying N's. Comparison of $\varpi_i(\theta)$ in the pinned region to the velocity of the moving boundary reveals that the particles in the pinned region lag behind the moving boundary for low values of N, but approach the speed of the boundary at high N, as shown in Fig. 3(b). Therefore, the average angular velocity of the cluster is dictated by the interaction of the particles in the pinned region with the container's wall, in analogy to the slip condition s of the single-particle model.
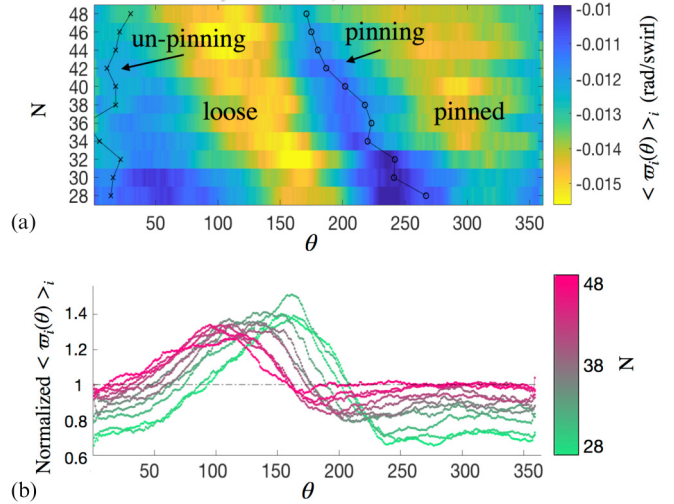

FIG. 3. (a) Experimental average particle angular velocity $\langle \varpi_i^M(\theta) \rangle_i$ about the cluster's center of mass, as a function of θ and N. In the loose region, $\varpi_i(\theta)$ increases and decreases in a quantitatively similar manner for all values of N, with the only difference being the location on the dish at which this peak occurs. However, in the pinned region, the average value of $|\varpi_i(\theta)|$ consistently increases with increasing N. Plotted in black are the average locations at which particles enter the pinned and loose regions. Note that the apparent decrease of $|\langle \varpi_i^M(\theta) \rangle_i|$ in the transition regions is an artifact of the oblong shape of the particle cluster. The transition regions occur at higher distances from the center, but the linear velocity of the particles during the transition regions does not change much. (b) Average experimental angular velocity of particles circling the dish, normalized with respect to the angular velocity of the wall about the cluster's center of mass. This is done by dividing $\langle \varpi_i(\theta) \rangle_i$ by the angular velocity of the boundary around the cluster's center of mass, a function of θ since the center of mass is not at C. At low N, a normalized velocity <1 in the pinned region indicates that those particles are traveling slower than the dish wall. As N is increased, the normalized velocity of particles in the pinned region approaches 1, meaning the particles are moving at the velocity of the wall.

D. Particle cluster slip parameter

Indeed, it is possible to define an analogous slip parameter for the swirling cluster,

$$s = \frac{\gamma}{\gamma_c} = \frac{\varpi_M}{\omega} \frac{P_{\mathrm{ball}}}{P_{\mathrm{cont}}}, \tag{2}$$

where the radii of the rigid ball and container have been replaced by their respective perimeters, P_{ball} and P_{cont}, to account for the deformability of the cluster. The particles considered for this calculation are only the ones along the perimeter of the cluster. Accordingly, the slip parameter of the pinned particles in our system increases from approximately 0.5 at $N = 25$ to nearly 1 at the highest values of N, as shown in Fig. 4(a). Similarly, our experimentally swirled cluster behaves increasingly similarly to a model particle with no-slip boundary conditions as N is increased, as shown in Fig. 1(b), confirming that counterrotation is due to increasingly no-slip boundary conditions.
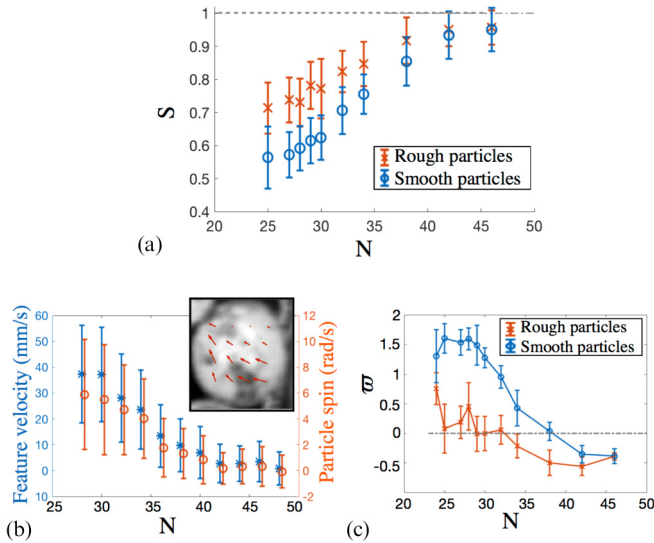
FIG. 4. Experimental data. (a) The slip parameter s is defined as the slip conditions between the particle cluster and the container wall. The value of s of the particles in the pinned region approaches 1 as N is increased, corresponding to the pinned region particles moving more coherently with the moving wall. Additionally, the slip parameter s of roughened particles along the wall of the pinned region is closer to 1 (nonslip conditions) than for smoother particles, meaning that roughened particles also move more coherently with the moving wall in the pinned region. (b) The local rotation, as well as variability in rotation behavior, of individual particles along the wall in the pinned area decreases with increasing N, a result of increasing frustration between the particles. Inset shows snapshot of a particle with overlaid particle image velocimetry (PIV) vectors. We use PIV on the surface features of the particles to determine overall feature velocity (blue) and particle spinning about a vertical axis through its own center (orange). (c) Particles with roughened surfaces, and therefore increased friction, transition to counterrotation at a lower N than for smoother particles.

E. Pinned region particle dynamics

At low N, the particles at the wall in the pinned region are free to spin and roll locally, falling behind the moving wall and effectively reducing the particle cluster's friction with the container. This effective slip of the cluster on the wall corresponds to $s \ll 1$, and the cluster rotates in the laboratory frame. As N increases, the particles in the pinned region pack together more tightly, and friction between the particles dominates. When interparticle friction is strong between two contacting particles, they must spin about their own axes in opposite directions, dictating antiferromagnetic-like interactions for spinning. For sixfold packing, as we often see in the pinned region, this results in geometric frustration, prohibiting any of the particles from rolling or spinning freely at high N, as shown in Fig. 4(b). Similarly, particles in strong contact cannot advance as a tight single file due to geometric frustration and can only roll on the ground side by side. The inability to individually roll causes the particles to effectively stick to the container wall, resulting in less effective wall slip ($s \approx 1$). Therefore, the increased frictional effects at high N cause the dense particle cluster to roll, or rather treadmill, on the container wall, resulting in counterrotation.

F. Friction affects counterrotation

If friction is indeed what drives counterrotation, one would expect that increased frictional effects achieved by alternative means would also promote counterrotation. Indeed, sandpaper-roughened particles transition to counterrotation at $N = 28$ as compared to $N = 36$ for smooth particles, as shown in Fig. 4(c), confirming the importance of friction to counterrotation. Furthermore, the calculated slip parameter s for the roughened particles is consistently closer to 1 than for the smooth particles, as shown in Fig. 4(a), affirming that counterrotation is associated with increasingly no-slip boundary conditions.

II. SIMULATIONS

Further experimentally testing the importance of friction to counterrotation is a challenge since it is difficult to systematically fine-tune or completely eliminate the friction. We therefore turn to numerical simulations, which offer the unique advantage of adjusting physical constants that are impossible to change experimentally.

We numerically simulate a system where N two-dimensional disks with radius $r = 1$ are swirled in a circular container with radius $R = 8.6$, as shown in Fig. 5(a). The container is translated around a polygonal path with 30 sides and amplitude $A = 0.96$, approximating a circle while allowing particle-wall collisions to be solved analytically. The behavior of the particles is simulated using an event-driven method, with the particles' linear and angular velocities updated every collision and otherwise determined via Newton's equations. Such a method allows us to exactly solve the dynamics up to floating-point precision, with the minimal number of parameters and ingredients in the model. Collisions are perfectly elastic in the normal direction and in the tangential direction are subject to frictional impulses derived from Coulomb's law, using a coefficient of friction μ_d for particle-particle collisions and μ_w for particle-wall collisions [19] (see the Supplemental Material [17]).

The average angular velocity ϖ for the simulations is qualitatively similar to those measured in the experiments, exhibiting a rotation-counterrotation transition with increasing N, as shown in Fig. 5(b). The M-frame density histograms and relative angular velocities are also qualitatively similar to those of the experiment, as shown in Figs. 5(c) and 5(d). The qualitative similarity between the experiments and simulations is striking, given that the simulations are significantly simplified; notably, there is no friction with the substrate, no three-dimensional rolling effects, and no normal damping during collisions, so the disks never actually stick to each other. Therefore, these additional factors cannot be critical for observing the transition.

A. Tuning disk-wall and disk-disk frictions

If the transition from rotation to counterrotation is indeed driven by friction both between the disks and with the container, then decreasing those frictions would require more disks to achieve the same effective friction and therefore the counterrotation transition should occur at a higher N. Indeed, decreased disk-disk and disk-wall friction cause the

(a)   (b)

(c)

rotation: N=28   counterrotation: N=48

(d)

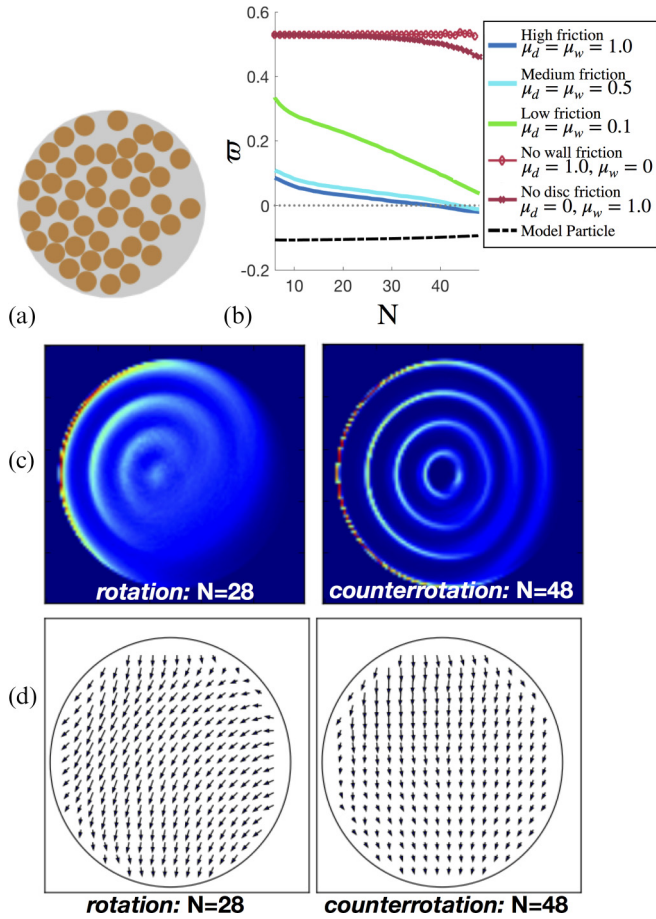rotation: N=28   counterrotation: N=48

FIG. 5. Simulations. (a) Snapshot of the simulated disks. (b) The particle cluster transitions from rotation to counterrotation as N is increased when friction is present. This rotation-counterrotation transition point occurs at higher N when friction is decreased. When either disk-disk or disk-wall friction is completely eliminated, the system never transitions to counterrotation. Here "high friction" is $\mu_d = \mu_w = 1.0$, "medium friction" is $\mu_d = \mu_w = 0.5$, and "low friction" is $\mu_d = \mu_w = 0.1$. When one friction is completely turned off, the other friction is set to 1.0. (c) Density histogram of the disks for a rotating ($N = 28$, left) and counterrotating ($N = 48$, right) case. (d) Quiver plots showing the average local disk velocity deviation from the container for a rotating ($N = 28$, left) and counterrotating ($N = 48$, right) case.

counterrotation transition to occur at higher N, as shown in Fig. 5(b). Furthermore, completely turning off friction should eliminate the transition to counterrotation. We test these two cases separately.

B. Turning off disk-wall friction

We first test the importance of boundary friction by eliminating disk-wall friction ($\mu_w = 0$), resulting in a frictionless boundary that serves only to contain the disks via hard-core-like elastic interactions. The disks may still frustrate each others' abilities to spin about their own axes, but without wall friction the disks are not encouraged to rotate commensurately with the wall. In the laboratory frame, the cluster of disks behaves as a solid-like unit sloshing around the container

without any internal individual spinning (see Supplemental Material [17]). The angular velocity of the cluster therefore remains at that of the container regardless of N, as shown in Fig. 5(b). In the M frame, the disks form a rim at the boundary of the container with very little internal movement (Supplemental Material [17]). The steady state of these particles arises from the centrifugal force pushing particles to the wall, much like sand settling under gravity. However, without additional forcing from the wall, the angular velocity of the cluster cannot change, so the system never transitions to counterrotation, verifying that disk-wall friction is critical to induce counterrotation.

C. Turning off disk-disk friction

Next, we separately test the importance of disk-disk friction by eliminating it ($\mu_d = 0$) and bringing back disk-wall friction. In this system, the outer disks are accelerated by frictional collisions with the wall and spin about their own axes quickly. However, with no disk-disk friction, none of this spinning is transferred to the inner disks except through particle exchanges, so individual disks spin with no coherence. The cluster of disks is loose and gaslike, unlike the rigid body appearance of the cluster when all friction is present (Supplemental Material [17]). With no disk-disk friction, the average angular velocity remains close to the container velocity, except at very high N, where it drops slightly. The system never transitions to counterrotation, verifying that disk-disk friction is also critical to induce counterrotation.

III. CONCLUSIONS

In conclusion, we perform experiments and numerical simulations of swirled granular media and identify the minimal ingredients for the particles and their interactions necessary to induce counterrotation. We use a frame of reference in which the dynamics of swirled granular media are at steady state, the M frame. In this frame of reference, we introduce a minimal model, where the granular cluster is replaced by a single ball within a rotating drum. This system can capture the observed dynamics by only tuning the amount of slip s that the ball experiences with the wall of the rotating drum. When the ball experiences strong slip on the wall ($s \ll 1$), the system rotates in the laboratory frame, while minimal slip ($s \approx 1$) corresponds to counterrotation in the laboratory frame. In the granular system, $s \ll 1$ is the result of individual particles falling behind the moving wall while rolling freely along the wall and the ground, acting as bearings for the particle cluster against the wall. This is generally true at low N when the effective friction is minimal, and corresponds to rotation in the laboratory frame. On the other hand, $s \approx 1$ occurs when the individual particles along the wall move with the wall due to high packing densities and geometric frustration. This is generally true for densely packed particles at high N. Particle-particle friction prevents closely packed particles from spinning and rolling freely, converting the particle ensemble into a solid-like cluster. At the same time, particle-wall friction causes that solid-like cluster of particles to stick to the wall, causing the overall cluster to roll commensurately along the wall and counterrotate, much like a pancake in a swirling pan.

Our investigation has considered the dynamics of discrete particles but it would be interesting to model the system with continuum equations, coupling internal spinning to a continuum notion of vorticity. Such equations have modeled related systems [20–22] and could perhaps give insight into the sensitive interplay among pressure, vorticity, friction, and external forcing that leads to counterrotation. While our system is more complicated than the others that have been studied as it has no additional symmetries that lead to simplified equations, one could still study these equations numerically in the M frame where the external forces are stationary.

In our swirling system, the large-scale translation locally drives individual particles to roll on the ground and spin on their neighbors and the boundary. The individual particles then interact with each other via frictional collisions, causing the motion of the particles to eventually coalesce into system-size rotation or counterrotation. In addition to the swirling container and rotating drum systems, the behavior associated with interacting, individually driven particles can give rise to phase changes and bifurcations in other physical systems. Several studies have shown that interactions between actively moving or rotating objects, both self-propelled and system-scale driven, can lead to collective angular momentum changes and rich phase behaviors [4,5,21–26]. Specifically, in our system the interaction is particle friction and geometric frustration. Particle-particle rolling frustration is likely responsible for the rolling-jamming transition, resulting in an apparent discontinuous jump in effective friction when sheared layers of spherical marbles exceed a critical thickness [27]. The transition to solid-like behavior in these systems is driven by the inability of contacting particles to cospin or roll in line, distinct from solid-like behavior that is achieved via jamming [28,29] or rigidity percolation [30].

Finally, our observation that the transition to counterrotation can be manipulated by roughening the particles inspires a speculative but interesting analogy with the transition to turbulence in pipe flow, where a roughness-dependent transition has also been observed [31]. However, unlike pipe turbulence, it is not clear if the transition to counterrotation of swirling particles exhibits a true critical phenomenon.

[1] M. G. Shats, H. Xia, and H. Punzmann, Phys. Rev. E **71**, 046409 (2005).

[2] H. Xia, D. Byrne, G. Falkovich, and M. Shats, Nat. Phys. **7**, 321 (2011).

[3] A. Souslov, B. C. van Zuiden, B. Bartolo, and V. Vitelli, Nat. Phys. **13**, 1091 (2017).

[4] E. Lushi, H. Wioland, and R. E. Goldstein, Proc. Natl. Acad. Sci. USA **111**, 9733 (2014).

[5] H. Wioland, E. Lushi, and R. E. Goldstein, New J. Phys. **18**, 075002 (2016).

[6] A. Feltrup, K. Huang, C. Kruelle, and I. Rehberg, Eur. Phys. J.: Spec. Top. **179**, 19 (2009).

[7] M. A. Scherer, K. Kötter, M. Markus, E. Goles, and I. Rehberg, Phys. Rev. E **61**, 4069 (2000).

[8] T. Yokoyama, K. Tamura, H. Usui, and G. Jimbo, in *Proceedings of the Eighth European Symposium on Comminution, Stockholm, 1994* (Elsevier, Amsterdam, 1996), pp. 413–424.

[9] M. A. Scherer, V. Buchholtz, T. Pöschel, and I. Rehberg, Phys. Rev. E **54**, 4560(R) (1996).

[10] D. Kumar, N. Nitsure, S. Bhattacharya, and S. Ghosh, Proc. Natl. Acad. Sci. USA **112**, 11443 (2015).

[11] M. A. Scherer, T. Mahr, A. Engel, and I. Rehberg, Phys. Rev. E **58**, 6061 (1998).

[12] O. Zik and J. Stavans, Europhys. Lett. **16**, 255 (1991).

[13] S. Fauve, S. Douady, C. Laroche, and O. Thual, Phys. Scr. **T29**, 250 (1989).

[14] H. M. Jaeger, S. R. Nagel, and R. P. Behringer, Rev. Mod. Phys. **68**, 1259 (1996).

[15] D. Bi, J. Zhang, B. Chakraborty, and R. P. Behringer, Nature (London) **480**, 355 (2011).

[16] T. S. Majmudar, M. Sperl, S. Luding, and R. P. Behringer, Phys. Rev. Lett. **98**, 058001 (2007).

[17] See Supplemental Material at http://link.aps.org/supplemental/10.1103/PhysRevE.100.012903 for a video including the swirling beads in both the laboratory frame and M frame both experimentally and numerically, details on the M-frame conversion, details on the calculation of particles in the "loose" and "pinned" regions, and details of the numerical simulation.

[18] L. D. Landau and E. M. Lifshitz, *Mechanics* (Butterworth-Heinemann, Oxford, 1976).

[19] Y. Wang and M. T. Mason, J. Appl. Mech. **59**, 635 (1992).

[20] J. S. Dahler and L. E. Scriven, Nature (London) **192**, 36 (1961).

[21] J.-C. Tsai, F. Ye, J. Rodriguez, J. P. Gollub, and T. C. Lubensky, Phys. Rev. Lett. **94**, 214301 (2005).

[22] B. C. van Zuiden, J. Paulose, W. T. M. Irvine, D. Bartolo, and V. Vitelli, Proc. Natl. Acad. Sci. USA **113**, 12919 (2016).

[23] N. H. P. Nguyen, D. Klotsa, M. Engel, and S. C. Glotzer, Phys. Rev. Lett. **112**, 075701 (2014).

[24] K. Yeo, E. Lushi, and P. M. Vlahovska, Phys. Rev. Lett. **114**, 188301 (2015).

[25] M. Workamp, G. Ramirez, K. E Daniels, and J. Dijksman, Soft Matter **14**, 5572 (2018).

[26] F. Moisy, J. Bouvard, and W. Herreman, Europhys. Lett. **122**, 34002 (2018).

[27] C. Marone, B. M. Carpenter, and P. Schiffer, Phys. Rev. Lett. **101**, 248001 (2008).

[28] I. Peters, S. Majumdar, and H. Jaeger, Nature (London) **532**, 214 (2016).

[29] P. Coussot, N. Roussel, S. Jarny, and H. Chanson, Phys. Fluids **17**, 011704 (2005).

[30] S. Alexander, Phys. Rep. **296**, 65 (1998).

[31] N. Goldenfeld, Phys. Rev. Lett. **96**, 044503 (2006).